VIP Hollow Nanostructures Very Important Paper

DOI: 10.1002/ange.201400226

Formation of $Ni_xCo_{3-x}S_4$ Hollow Nanoprisms with Enhanced Pseudocapacitive Properties

*Le Yu, Lei Zhang, Hao Bin Wu, and Xiong Wen (David) Lou**

Abstract: *Hollow nanostructures are of great interest for a wide variety of applications. Despite the great advances, synthesis of anisotropic hollow structures is still very challenging. In this work, we have developed a simple sacrificial template method to synthesize uniform $Ni_xCo_{3-x}S_4$ hollow nanoprisms with tunable composition. Tetragonal nanoprisms of nickel–cobalt acetate hydroxide precursors with controllable Ni/Co molar ratios are first synthesized and used as the sacrificial templates. After a sulfidation process with thioacetamide (TAA) in ethanol, the solid precursor prisms can be transformed into the corresponding $Ni_xCo_{3-x}S_4$ hollow nanoprisms with a well-defined hollow interior. The intriguing structural and compositional features are beneficial for electrochemical applications. Impressively, the resultant $Ni_xCo_{3-x}S_4$ hollow prisms manifest a high specific capacitance with enhanced cycling stability, making them potential electrode materials for supercapacitors.*

Hollow micro-/nanostructures are a unique class of functional materials with well-defined cavities and the chemical functionality of shell materials.[1] Their intriguing structural features, such as large surface area, low density, a kinetically favorable open structure, and surface permeability, endow hollow structures with great technological importance in a myriad of applications, including catalysis, drug delivery, gas sensors, and energy storage systems.[2] As a result, controllable fabrication of hollow nanomaterials with a complex composition and delicate morphological control becomes more and more fascinating and vital for both fundamental studies and practical applications.[1f,3]

Numerous efforts have been devoted to developing methods for the rational synthesis of various hollow structures, and great progress has been achieved.[1c,e] Among these endeavors, synthesis involving templates has been demonstrated to be the most versatile route to generate various hollow structures with a narrow size distribution.[1d] Nevertheless, the geometry of products obtained in practice is mostly spherical. In this regard, many novel approaches have been developed to synthesize hollow architectures with anisotropic shapes for noble metals, transition metal oxides, and sulfides, based on diverse principles such as galvanic replacement, chemical etching, the Kirkendall effect, self-assembly, and thermal decomposition, among others.[1b,4] Notwithstanding these advances, the development of non-spherical hollow structures is more challenging because of the less controllable coating around high-curvature surfaces and the deficiency of non-spherical templates.[1d] Besides the shape control, another important parameter lies in delicate control over the chemical composition of hollow nanostructures such as binary or even ternary metal oxides and sulfides. Above all, different materials with distinct physical and chemical properties could hardly be incorporated simultaneously into the synthesis process.[5] In addition, the indispensable mass relocation during the prolonged reactions may result in undesired secondary phase formation or phase separation.[5,6] To circumvent these difficulties, Oh and coworkers recently reported a new mechanism based on the galvanic replacement reaction for the formation of hollow metal oxide nanocrystals, which allows the composition and morphology of oxide nanoparticles to be transformed in solution at low temperature.[1b] Also, we have recently developed a metal-organic-framework-derived method to synthesize hollow structures with designed compositions by the participation of various conjugate bases of metal-oxide-based weak acids.[3b] Despite the advances, it is challenging to extend these interesting templated strategies to other materials systems for different applications.

Recently, extensive research efforts have been devoted to the development of transition-metal sulfides in view of their outstanding properties in various applications.[7] In particular, ternary Ni–Co sulfides have attracted increasing attention as a new class of electrode materials in supercapacitors (SCs) with high electrochemical activity.[8] Moreover, Ni–Co sulfides may exhibit much higher conductivity than corresponding ternary Ni–Co oxides due to the lower band gap.[8b] It would therefore be desirable to synthesize ternary Ni–Co sulfides hollow structures and explore their electrochemical properties.[9]

Herein, we report a facile self-templating strategy to fabricate ternary $Ni_xCo_{3-x}S_4$ hollow nanoprisms by sulfidizing nickel–cobalt acetate hydroxide precursors with thioacetamide (TAA) in ethanol. This self-templated synthesis offers the additional possibility of engineering nanoprisms with a tunable hollow interior and chemical composition by tailoring the Ni/Co molar ratio of the precursors. Impressively, the as-obtained hollow prisms manifest high specific capacitance with enhanced cycling stability, making them potential electrode materials for SCs.

The synthetic strategy for anisotropic $Ni_xCo_{3-x}S_4$ hollow nanoprisms is shown in Figure 1 (see the Supporting Information for a detailed synthesis). We first developed a modified precipitation method to obtain highly uniform nickel–cobalt

[*] L. Yu, Dr. L. Zhang, H. B. Wu, Prof. X. W. Lou
School of Chemical and Biomedical Engineering, Nanyang Technological University, 62 Nanyang Drive, 637459 (Singapore)
E-mail: xwlou@ntu.edu.sg
Homepage: http://www.ntu.edu.sg/home/xwlou/

Supporting information for this article is available on the WWW under http://dx.doi.org/10.1002/anie.201400226.

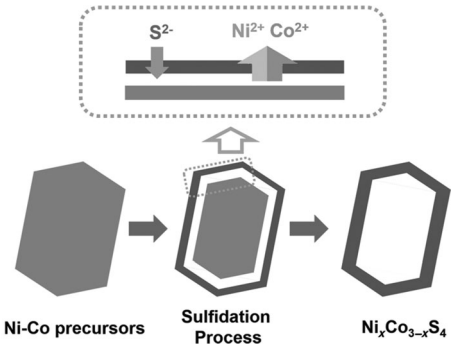

Figure 1. The formation of $Ni_xCo_{3-x}S_4$ hollow prisms from Ni–Co precursors by a diffusion-controlled process.

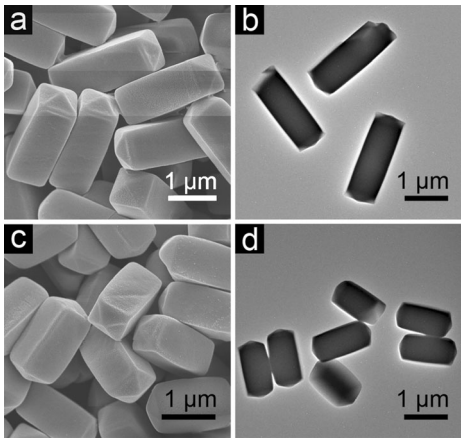

Figure 2. FESEM (a, c) and TEM (b, d) images of Ni–Co precursors: a, b) $NiCo_2$-pre; c, d) Ni_2Co-pre.

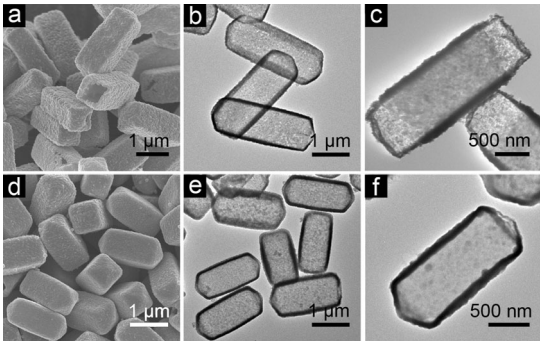

Figure 3. FESEM (a, d) and TEM (b, e) images of $NiCo_2S_4$ (a, b) and Ni_2CoS_4 (d, e) hollow prisms obtained after sulfidation process in ethanol. TEM images of $NiCo_2S_4$ (c) and Ni_2CoS_4 (f) hollow prisms annealed in nitrogen at 350 °C.

acetate hydroxide nanoprisms as the precursors.[10] Using TAA as the sulfur source, the solid precursors can be chemically transformed into $Ni_xCo_{3-x}S_4$ nanoprisms with well-defined hollow interior. Moreover, the evolution of hollow structures can be ascribed to the diffusion effect, which is widely employed to create interior voids for metal sulfides.[1a,11] Specifically, during the sulfidation process, sulfide ions released from TAA upon hydrolyzation react with metal ions to form a thin layer of Ni–Co sulfides, which acts as a physical barrier to hinder a direct chemical reaction between outside sulfide ions and inner metal-ion species. Therefore, further reaction depends on the relative diffusion of metal or sulfide ions through this newly formed sulfide layer. Owing to their smaller sizes, the outward diffusion of cationic species becomes dominant compared to the inward diffusion of anionic ones. As a result, the sulfidation reactions mainly take place on the preformed shell, and the hollow interior is finally formed. Importantly, this strategy can be applied successfully to all Ni–Co precursors with different Ni/Co molar ratios.

The morphology of Ni–Co precursors with Ni/Co molar ratios of 1:2 and 2:1 (denoted as $NiCo_2$-pre and Ni_2Co-pre, respectively) was first examined by field-emission scanning electron microscopy (FESEM) and transmission electron microscopy (TEM). The panoramic FESEM images show that these Ni–Co precursors are composed of highly uniform nanoprisms without impurity (Supporting Information, Figure S1). The magnified FESEM images (Figure 2 a,c) reveal that each tetragonal nanoprism has a pyramid-shaped apex at both ends with a rather smooth surface over the whole particle. As shown in Figure 2 b,d, TEM images of highly dispersed Ni–Co precursors have uniform contrast, clearly indicating their solid and dense nature. The $NiCo_2$-pre prisms are around 1.4 μm in length and 500 nm in width, whereas the Ni_2Co-pre sample consists entirely of shorter prisms with a length about 1.0 μm. The phase composition of Ni–Co precursors was investigated by X-ray diffraction (XRD; Figure S2 a). The XRD pattern could be assigned to a tetragonal nickel–cobalt acetate hydroxide phase, $(Ni,Co)_5(OH)_2(CH_3COO)_8{\cdot}2H_2O$, although the exact crystal structure remains unsolved.[10]

After sulfidation treatment in TAA solution, the overall nanoprism morphology of these Ni–Co precursors is well inherited by the Ni–Co sulfide hollow nanoprisms with a rough surface, as shown in Figure 3 a,d. The hollow interior and primary nanoparticles can be discerned unambiguously from some cracked hollow prisms. TEM study provides further insight into the hollow interior and detailed structure of the as-obtained nanoprisms. In agreement with FESEM observations, the well-defined inner cavities of highly uniform prisms are clearly elucidated by the sharp contrast between the center and the edge (Figure 3 b,e). The shell structure of Ni–Co sulfides with a uniform thickness (ca. 30–50 nm) is robust enough to endure the solvothermal reaction and subsequent processing. The complete phase conversion is corroborated by XRD analysis. The sulfidized sample from $NiCo_2$-pre turns out to be amorphous, with no characteristic peaks in the XRD pattern (Figure S2 b), whereas the prisms converted from Ni_2Co-pre could be identified as the cubic $CoNi_2S_4$ phase (JCPDS card no. 24-0334). Despite being very thin, the shells of these two samples possess good structural stability for withstanding the thermal annealing process in nitrogen atmosphere. After annealing, polycrystalline hollow prisms were obtained without apparent deformation in appearance, as revealed by TEM examination (Figure 3 c,f). From the XRD patterns (Figure S3), the crystallographic phase of the annealed samples can be identified as $NiCo_2S_4$

(JCPDS card no. 20-0782; space group: *Fd3m* (227); $a = b = c = 9.387$ Å) or $CoNi_2S_4$ (JCPDS card no. 24-0334; space group: *Fd3m* (227); $a = b = c = 9.428$ Å) with very similar cubic structures. No additional signals from possible impurities were detected, indicating the high purity of the products. From the high-resolution TEM images (Figure S4), the lattice fringes with interplanar distances of approximately 0.28 nm and 0.54 nm can be readily indexed to the (311) planes of $NiCo_2S_4$ and the (111) planes of Ni_2CoS_4, respectively. The samples were further characterized by energy-dispersive X-ray spectroscopy (EDX; Figure S5), which indicates that the Ni/Co atomic ratios of the hollow prisms from $NiCo_2$-pre and Ni_2Co-pre are about 1:2.75 and 1.63:1, respectively. It could be hypothesized that it is more difficult for Ni^{2+} ions to precipitate in ethanol, compared to Co^{2+} ions. For convenience, we still denote these two samples as $NiCo_2S_4$ and Ni_2CoS_4. As determined by N_2 sorption measurements (Figure S6), the $NiCo_2S_4$ and Ni_2CoS_4 hollow prisms possess Brunauer–Emmett–Teller (BET) specific surface areas of 30.0 and 22.5 $m^2 g^{-1}$, respectively, with pore sizes mostly below 10 nm. In addition, thermogravimetric analysis (TGA; Figure S7) reveals no apparent thermal decomposition below 400 °C during the annealing process in N_2 flow for the crystallized $NiCo_2S_4$ and Ni_2CoS_4 hollow prisms.

The shape and composition of Ni–Co precursors can be further tailored by altering the Ni/Co molar ratio in the starting materials. FESEM images (Figure S8) indicate that corresponding $Ni_xCo_{3-x}S_4$ hollow prisms can be easily generated from different Ni–Co precursors after an identical sulfidation treatment. This offers the potential to optimize the performance of these functional materials. The corresponding EDX results for these $Ni_xCo_{3-x}S_4$ hollow prisms (Figure S9) indicate that the Ni/Co atomic ratios are close to the precursor molar ratios. Co-precursor particles and corresponding CoS_x hollow structures can also be obtained (Figure S10), but Ni-precursor particles cannot be generated under similar synthesis conditions.

The electrochemical performance of these $Ni_xCo_{3-x}S_4$ hollow prisms is investigated as electrodes for SCs. The representative cyclic voltammetry (CV) curves at a constant scan rate of 2 mV s^{-1} in a potential window of 0–0.55 V for the $NiCo_2S_4$ and Ni_2CoS_4 hollow prisms are presented in Figure 4a. Interestingly, two pronounced pairs of well-defined redox peaks related to reversible Faradaic reactions of MS/MSOH and MSOH/MSO (M = Ni and Co species) can be clearly observed in the CV profiles, demonstrating their pseudo-capacitive characteristics.[8b,12] Comparing these two CV curves for $Ni_xCo_{3-x}S_4$ with different Ni/Co ratios, the first anodic peak in the CV curves shifts to a more positive potential as Ni content in the sample increases.[13] In addition, the peak current of the first pair for Ni_2CoS_4 is much higher than that for $NiCo_2S_4$. This pair of redox peaks in both CV curves might be attributed to Faradaic reactions of $Ni_xCo_{3-x}S_4$ to form NiSOH and CoSOH.[14] Whereas, the second pair at more positive potential might be mainly associated with the redox reaction between CoSOH and CoSO. This might account for the observation that the peak current of this pair is much higher for $NiCo_2S_4$. Furthermore, with the increase in sweep rate from 2 to 50 mV s^{-1}, the general shape

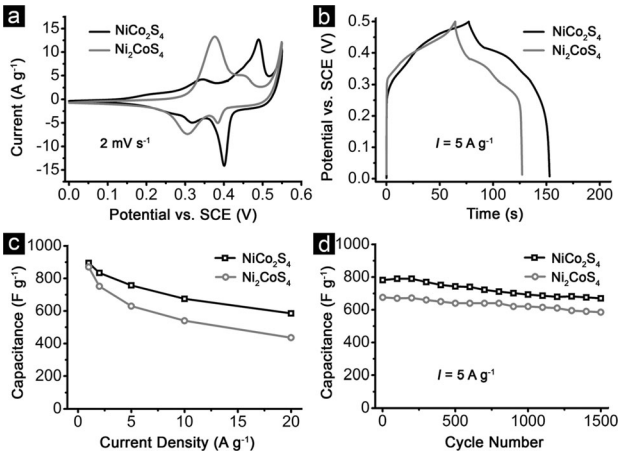

Figure 4. Electrochemical properties of $NiCo_2S_4$ and Ni_2CoS_4 hollow prisms: a) CV curves at a scan rate of 2 mV s^{-1}; b) CP plots; c) capacitance as a function of current density; d) cycling performance at a constant current density of 5 A g^{-1}.

of all CV curves evolves insignificantly with a slight shift in the peak position (Figures S11a and S12a). Figure 4b shows the galvanostatic charge/discharge measurements performed in the voltage range between 0 and 0.5 V (vs. SCE) at a constant current density of 5 A g^{-1}. As can be seen, two distinct voltage plateaus are well manifested in the charge and discharge curves for both samples, which is consistent with the CV measurements. The current-density dependence of specific capacitance is calculated from chronopotentiometry (CP) curves (Figures S11b and S12b) and plotted in Figure 4c. These CP curves are nearly symmetrical, indicating good electrochemical capacitive characteristics and excellent reversibility of the redox reactions for these $Ni_xCo_{3-x}S_4$ hollow prisms. Impressively, the $NiCo_2S_4$ hollow prisms deliver very high capacitance of 895.2, 834.4, 757.4, 674.8, and 585.2 F g^{-1} at current densities of 1, 2, 5, 10, and 20 A g^{-1}, respectively, compared to 870–436 F g^{-1} at the same current density range of 1–20 A g^{-1} for the Ni_2CoS_4 hollow prisms. This suggests that about 65.4% of the capacitance for $NiCo_2S_4$ hollow prisms is still retained when the current density is increased from 1 to 20 A g^{-1}. The enhancement in electrochemical capacitance of the as-obtained $NiCo_2S_4$ hollow prisms might be ascribed to the larger surface area, which endows more active sites for electrochemical reactions and more efficient penetration of electrolyte into the electroactive materials. In addition, the cycling stability is also evaluated by the repeated charging–discharging measurement at a constant current density of 5 A g^{-1}. As shown in Figure 4d, both $NiCo_2S_4$ and Ni_2CoS_4 hollow prisms possess high electrochemical stability for a long cycle life. For $NiCo_2S_4$ hollow prisms, the specific capacitance is about 782 F g^{-1} in the first cycle, and it gradually decreases to 670 F g^{-1} after 1500 repeating cycles with a total capacitance loss of about 14.3%. Meanwhile, the specific capacitance of the Ni_2CoS_4 hollow prisms decreases from 676 to 585 F g^{-1}, with capacitance retention of 86.5% after continuous cycling for 1500 cycles. The supercapacitive performance of these $Ni_xCo_{3-x}S_4$ hollow prisms is superior to that of many binary or ternary nickel-

and cobalt-based sulfides.[8–9,15] The electrochemical properties of $Ni_xCo_{3-x}S_4$ hollow prisms are much better than that of CoS_x hollow prisms (Figure S13). Such desirable pseudocapacitive performance of $Ni_xCo_{3-x}S_4$ hollow prisms might be attributed to their unique structural and compositional features. In particular, the void space in the interior together with the permeable thin walls provides sufficient electroactive sites and electrolyte–electrode interface for fast diffusion and reaction.[16]

In summary, we have developed a facile and efficient self-templating conversion method to synthesize $Ni_xCo_{3-x}S_4$ hollow prisms with a tunable hollow interior and chemical composition. After a mild sulfidation process with thioacetamide (TAA), the solid tetragonal prisms of nickel–cobalt acetate hydroxide precursors can be chemically transformed into corresponding Ni–Co sulfide prisms with a well-defined hollow interior. The as-synthesized $Ni_xCo_{3-x}S_4$ hollow prisms exhibit remarkable electrochemical performance as electrodes for high-performance supercapacitors. Specifically, these hollow prisms can deliver a high specific capacitance of 895.2 $F g^{-1}$ at 1 $A g^{-1}$, with desirable rate performance and good capacitance retention after 1500 cycles.

Received: January 9, 2014
Published online: March 3, 2014

Keywords: cobalt · nanostructures · nickel · prisms · supercapacitors

[1] a) Y. D. Yin, R. M. Rioux, C. K. Erdonmez, S. Hughes, G. A. Somorjai, A. P. Alivisatos, *Science* **2004**, *304*, 711; b) M. H. Oh, T. Yu, S. H. Yu, B. Lim, K. T. Ko, M. G. Willinger, D. H. Seo, B. H. Kim, M. G. Cho, J. H. Park, K. Kang, Y. E. Sung, N. Pinna, T. Hyeon, *Science* **2013**, *340*, 964; c) X. W. Lou, L. A. Archer, Z. C. Yang, *Adv. Mater.* **2008**, *20*, 3987; d) X. Y. Lai, J. E. Halpert, D. Wang, *Energy Environ. Sci.* **2012**, *5*, 5604; e) J. Hu, M. Chen, X. S. Fang, L. W. Wu, *Chem. Soc. Rev.* **2011**, *40*, 5472; f) J. W. Nai, Y. Tian, X. Guan, L. Guo, *J. Am. Chem. Soc.* **2013**, *135*, 16082; g) Z. H. Dong, X. Y. Lai, J. E. Halpert, N. L. Yang, L. X. Yi, J. Zhai, D. Wang, Z. Y. Tang, L. Jiang, *Adv. Mater.* **2012**, *24*, 1046; h) J. Liu, H. Q. Yang, F. Kleitz, Z. G. Chen, T. Y. Yang, E. Strounina, G. Q. Lu, S. Z. Qiao, *Adv. Funct. Mater.* **2012**, *22*, 591.

[2] a) X. L. Pan, Z. L. Fan, W. Chen, Y. J. Ding, H. Y. Luo, X. H. Bao, *Nat. Mater.* **2007**, *6*, 507; b) B. Y. Xia, H. B. Wu, X. Wang, X. W. Lou, *J. Am. Chem. Soc.* **2012**, *134*, 13934; c) Y. F. Zhu, J. L. Shi, W. H. Shen, X. P. Dong, J. W. Feng, M. L. Ruan, Y. S. Li, *Angew. Chem.* **2005**, *117*, 5213; *Angew. Chem. Int. Ed.* **2005**, *44*, 5083; d) J. Liu, S. Z. Qiao, J. S. Chen, X. W. Lou, X. R. Xing, G. Q. Lu, *Chem. Commun.* **2011**, *47*, 12578; e) J. H. Lee, *Sens. Actuators B* **2009**, *140*, 319; f) K. T. Lee, Y. S. Jung, S. M. Oh, *J. Am. Chem. Soc.* **2003**, *125*, 5652; g) L. Yu, H. B. Wu, X. W. Lou, *Adv. Mater.* **2013**, *25*, 2296.

[3] a) M. Ibanez, A. Cabot, *Science* **2013**, *340*, 935; b) L. Zhang, H. B. Wu, X. W. Lou, *J. Am. Chem. Soc.* **2013**, *135*, 10664.

[4] a) S. E. Skrabalak, J. Y. Chen, Y. G. Sun, X. M. Lu, L. Au, C. M. Cobley, Y. N. Xia, *Acc. Chem. Res.* **2008**, *41*, 1587; b) Z. Y. Wang, D. Y. Luan, C. M. Li, F. B. Su, S. Madhavi, F. Y. C. Boey, X. W. Lou, *J. Am. Chem. Soc.* **2010**, *132*, 16271; c) H. J. Fan, U. Gosele, M. Zacharias, *Small* **2007**, *3*, 1660; d) G. Q. Zhang, L. Yu, H. B. Wu, H. E. Hoster, X. W. Lou, *Adv. Mater.* **2012**, *24*, 4609.

[5] L. Zhou, D. Y. Zhao, X. W. Lou, *Angew. Chem.* **2012**, *124*, 243; *Angew. Chem. Int. Ed.* **2012**, *51*, 239.

[6] a) J. Li, H. C. Zeng, *J. Am. Chem. Soc.* **2007**, *129*, 15839; b) X. Wang, Y. T. Zhong, T. Y. Zhai, Y. F. Guo, S. M. Chen, Y. Ma, J. N. Yao, Y. Bando, D. Golberg, *J. Mater. Chem.* **2011**, *21*, 17680.

[7] a) C. W. Kung, H. W. Chen, C. Y. Lin, K. C. Huang, R. Vittal, K. C. Ho, *Acs Nano* **2012**, *6*, 7016; b) C. H. Lai, M. Y. Lu, L. J. Chen, *J. Mater. Chem.* **2012**, *22*, 19.

[8] a) S. J. Peng, L. L. Li, C. C. Li, H. T. Tan, R. Cai, H. Yu, S. Mhaisalkar, M. Srinivasan, S. Ramakrishna, Q. Y. Yan, *Chem. Commun.* **2013**, *49*, 10178; b) H. C. Chen, J. J. Jiang, L. Zhang, H. Z. Wan, T. Qi, D. D. Xia, *Nanoscale* **2013**, *5*, 8879.

[9] a) L. Zhang, H. B. Wu, X. W. Lou, *Chem. Commun.* **2012**, *48*, 6912; b) Q. H. Wang, L. F. Jiao, H. M. Du, Y. C. Si, Y. J. Wang, H. T. Yuan, *J. Mater. Chem.* **2012**, *22*, 21387; c) Z. S. Yang, C. Y. Chen, H. T. Chang, *J. Power Sources* **2011**, *196*, 7874; d) T. Zhu, Z. Y. Wang, S. J. Ding, J. S. Chen, X. W. Lou, *Rsc Adv.* **2011**, *1*, 397; e) S. J. Peng, L. L. Li, H. T. Tan, R. Cai, W. H. Shi, C. C. Li, S. Mhaisalkar, M. Srinivasan, S. Ramakrishna, Q. Y. Yan, *Adv. Funct. Mater.* **2014**, DOI: 10.1002/adfm.201303273.

[10] W. Du, R. M. Liu, Y. W. Jiang, Q. Y. Lu, Y. Z. Fan, F. Gao, *J. Power Sources* **2013**, *227*, 101.

[11] a) G. J. Xiao, Y. Zeng, Y. Y. Jiang, J. J. Ning, W. T. Zheng, B. B. Liu, X. D. Chen, G. T. Zou, B. Zou, *Small* **2013**, *9*, 793; b) H. L. Cao, X. F. Qian, C. Wang, X. D. Ma, J. Yin, Z. K. Zhu, *J. Am. Chem. Soc.* **2005**, *127*, 16024.

[12] L. Yu, G. Q. Zhang, C. Z. Yuan, X. W. Lou, *Chem. Commun.* **2013**, *49*, 137.

[13] L. Huang, D. C. Chen, Y. Ding, S. Feng, Z. L. Wang, M. L. Liu, *Nano Lett.* **2013**, *13*, 3135.

[14] a) L. Mei, T. Yang, C. Xu, M. Zhang, L. B. Chen, Q. H. Li, T. H. Wang, *Nano Energy* **2014**, *3*, 36; b) H. Z. Wan, J. J. Jiang, J. W. Yu, K. Xu, L. Miao, L. Zhang, H. C. Chen, Y. J. Ruan, *CrystEngComm* **2013**, *15*, 7649.

[15] W. J. Zhou, X. H. Cao, Z. Y. Zeng, W. H. Shi, Y. Y. Zhu, Q. Y. Yan, H. Liu, J. Y. Wang, H. Zhang, *Energy Environ. Sci.* **2013**, *6*, 2216.

[16] a) Q. Lu, J. G. G. Chen, J. Q. Xiao, *Angew. Chem.* **2013**, *125*, 1932; *Angew. Chem. Int. Ed.* **2013**, *52*, 1882; b) C. Z. Yuan, H. B. Wu, Y. Xie, X. W. Lou, *Angew. Chem.* **2014**, *126*, 1512; *Angew. Chem. Int. Ed.* **2014**, *53*, 1488.

